Pilot Study to Diagnose Nonalcoholic Steatohepatitis With Dynamic ^{18}F-FDG PET

Souvik Sarkar[1]
Michael T. Corwin[2]
Kristin A. Olson[3]
Susan L. Stewart[4]
Chung-Heng Liu[1]
Ramsey D. Badawi[2]
Guobao Wang[2]

OBJECTIVE. Nonalcoholic fatty liver disease (NAFLD) and nonalcoholic steatohepatitis (NASH) are major causes of chronic liver disease characterized by steatosis, inflammation, and fibrosis. Diagnosis of inflammation is limited by the need for liver biopsy. Dynamic PET with the widely used radiotracer ^{18}F-FDG provides a novel method for evaluating spatial and temporal changes in liver inflammation.

MATERIALS AND METHODS. Patients with NAFLD or NASH underwent dynamic FDG PET and MRI within 6 months of undergoing liver biopsy. Liver time-activity curves were extracted to estimate kinetic parameters representing various rate constants of FDG transport using tracer kinetic modeling. Liver biopsy specimens were scored on the basis of NASH Clinical Research Network criteria.

RESULTS. This pilot study included 22 patients, 14 of whom were women. Patient age ranged from 18 to 70 years, and the mean body mass index (weight in kilograms divided by the square of height in meters) was 33.2 (range, 24–43.1). The K_1 value, which represents the rate of FDG transport from blood to hepatic tissue, was significantly correlated with inflammation ($r = -0.7284$; $p = 0.0001$) and the overall NAFLD activity score (NAS; $r = -0.6750$; $p = 0.0006$). K_1 values were inversely related to the hepatic inflammation score and NAS. Although heterogeneity in K_1 values across eight liver segments was noted, distinct segregation existed among segmental K_1 values dependent on the histologic inflammation score ($p = 0.022$) or NAS ($p = 0.0091$). K_1 had a strong association with both inflammation (ROC AUC value, 0.88) and the NAS (ROC AUC value, 0.89), with $K_1 = 1.02$ (mL/min/mL) corresponding to a sensitivity and specificity of 93% and 88%, respectively, for the NAS.

CONCLUSION. Dynamic FDG PET with tracer kinetic modeling has the potential to determine liver inflammation in patients with NAFLD and NASH and can fill an essential gap in diagnosis.

Keywords: FDG, liver inflammation, nonalcoholic fatty liver disease, nonalcoholic steatohepatitis, PET

doi.org/10.2214/AJR.18.20012

Received April 18, 2018; accepted after revision August 6, 2018.

Based on presentations at the European Society for the Study of Liver Diseases 2017 annual meeting (Amsterdam, The Netherlands) and the American Association for the Study of Liver Diseases 2017 annual meeting (Washington, DC).

Supported by University of California, Davis, start-up funds to S. Sarkar and G. Wang and Collaborative for Diagnostic Innovation Grant to S. Sarkar.

[1]Department of Internal Medicine, Division of Gastroenterology and Hepatology, University of California, Davis, 4150 V St, PSSB 3500, Sacramento, CA 95817. Address correspondence to S. Sarkar (ssarkar@ucdavis.edu).

[2]Department of Radiology, University of California, Davis, Sacramento, CA.

[3]Department of Pathology and Laboratory Medicine, University of California, Davis, Sacramento, CA.

[4]Department of Public Health Sciences, Division of Biostatistics, University of California, Davis, Sacramento, CA.

Supplemental Data
Available online at www.ajronline.org.

AJR 2019; 212:529–537

0361–803X/19/2123–529

Fatty liver disease, or nonalcoholic fatty liver disease (NAFLD), is a national and global epidemic. NAFLD is characterized by a spectrum of liver pathologic findings ranging from fat deposition in the hepatocytes (steatosis) to florid inflammation (nonalcoholic steatohepatitis [NASH]), and fibrosis [1, 2]. Fibrosis remains the key determinant of worse disease outcome in patients with NAFLD [3]. Inflammation or NASH is the key driver of fibrosis [4], with an associated risk of progression to cirrhosis and its complications (i.e., portal hypertension and hepatocellular carcinoma). Multiple new therapeutic agents are being investigated in clinical trials with the key intent of achieving regression of fibrosis and reducing inflammation [4]. Unfortunately, tools for the detection of hepatic inflammation, which serves as one of the clinical endpoints for patient care, remain limited. Liver biopsy remains the current reference standard for the detection of hepatic inflammation and diagnosis of NASH [5, 6]. Biopsy, however, is limited by its invasiveness, in addition to associated serious complications, patient anxiety, patient discomfort, sampling errors, interobserver variability, and costs [7, 8]. Noninvasive tests, such as liver enzyme analysis or observation of a combination of serum biomarkers, have not shown promise [6]. Imaging modalities based on ultrasound or MRI are emerging as potential tools that have a high sensitivity for the detection of hepatic fat and fibrosis [9] but not for the diagnosis of inflammation, NASH, or a combination of these two conditions. Diagnosis of inflam-

mation or NASH is essential as newer therapeutic regimens become available to enable effective risk stratification and patient management [10, 11].

PET is a functional and molecular imaging modality that uses the widely accessible radiotracer ^{18}F-FDG. FDG PET is well known as an effective method for imaging glucose metabolism related to glycolysis in cells [12]. The current clinical use of FDG PET is mainly limited to static PET protocols that examine tracer spatial distribution at a late point in time (commonly 60 minutes after FDG injection), providing the standardized uptake value (SUV) as a semiquantitative measure of glucose utilization [13, 14]. Studies have shown the utility of static FDG PET for studying physiologic liver processes affected by obesity and NAFLD [15–18]. However, this static means of using FDG PET may not exploit its full potential in evaluating patients with NAFLD. Dynamic FDG PET acquires images showing FDG activity at multiple time points to monitor both spatial and temporal distributions, enabling the ability to exploit the kinetic characteristics of FDG uptake by tracer kinetic modeling [19]. These kinetic parameters derived from dynamic FDG PET represent the underlying molecular processes of the uptake and trapping of FDG in the liver that may better characterize the status of liver disease. Borra et al. [20] showed an inverse association between liver fat content and hepatic glucose uptake measured using FDG PET, whereas Iozzo et al. [18, 21] used dynamic FDG PET to show the effect of hyperinsulinemia on hepatic glucose uptake, revealing physiologic changes in overall hepatic glucose with alterations in metabolic states. Indeed, in nuclear cardiology, interest in the utility of dynamic FDG PET is growing [22], but data remain limited.

Although specific alterations in the individual kinetic parameters involved in glucose transport (such as phosphorylation, dephosphorylation, and overall hepatic glucose uptake) have been defined [16, 18, 20, 21], they have never been clearly evaluated in patients with fatty liver disease, especially in conjunction with histologic changes. The potential role of dynamic FDG PET in diagnosing NASH is thus explored in the current study in association with its histologic determinants. Furthermore, we used an in-house [23] kinetic modeling package to estimate kinetic parameters while applying correction for the dispersion effect caused by the dual blood supply. We hypothesize that changes in FDG kinetic parameters will correlate with changes in hepatic inflammation in patients with NAFLD and NASH, on the basis of liver biopsy findings. In addition, we also aim to explore the potential of dynamic FDG PET for imaging of liver inflammation, which may enable efficient clinical detection of the early stages of NASH.

Materials and Methods

Study Design and Population

The study is designed as a cross-sectional study of patients with fatty liver disease who have undergone or will undergo a liver biopsy. The institutional review board and the radiation use committee at the University of California, Davis, approved the study. The time window for the imaging studies ranged from 2 weeks (to allow time for any local postbiopsy inflammation to subside) to 6 months after liver biopsy was performed. The baseline clinical and laboratory values of the patients enrolled in the study were recorded. All patients also underwent MRI proton-density fat fraction (PDFF) to quantitate hepatic fat using MRI in accordance with well-established criteria [24]. MR elastography (MRE) was performed to evaluate liver stiffness as described elsewhere [25].

Inclusion and Exclusion Criteria

Patients older than 18 years who had a diagnosis of fatty liver disease, were undergoing liver biopsy, and were able to provide informed consent were eligible to enroll in the study. Pregnant patients, prisoners, and individuals with a history of alcohol abuse, chronic hepatitis B or C, or other chronic liver disease were excluded from the study. A history of any allergy to FDG or an inability to lie in the bed of the PET scanner for approximately 1 hour was considered a reason for exclusion from the study.

Study Objectives

The primary objective was to determine FDG PET kinetic parameters that correlate with histologic findings of hepatic inflammation. The secondary objective was to determine the distribution of hepatic inflammation.

Waist Circumference and Body Mass Index

A tape measure was used to determine the waist circumference using standard methods, and body mass index (BMI) was measured as weight in kilograms divided by the square of height in meters at the time that consent was given.

Medical Record Review

The study coordinators and a hepatologist performed a review of the medical records to document patient demographic characteristics, laboratory values, comorbidities, and medications. The presence of comorbidities (e.g., diabetes, hypertension, or hyperlipidemia) was determined on the basis of the diagnoses outlined in each patient's chart.

Liver Histologic Findings

A single expert pathologist scored the liver biopsy specimens in accordance with the histologic scoring system of the Nonalcoholic Steatohepatitis Clinical Research Network (NASH CRN) [26–28]. The NAFLD activity score (NAS) (combined scores for steatosis [grades 0–3], lobular inflammation [grades 0–3], and ballooning degeneration [grades 0–2]), as developed by the NASH CRN, was determined for the patients [27, 28]. A combined NAS of 4 or greater has been reported to correlate with the presence of NASH, whereas scores for lobular inflammation and ballooning degeneration are noted to represent hepatic inflammation [5, 27]. The sum of the lobular inflammation score and the ballooning degeneration score was deemed the hepatic inflammation score. A score of 3 or less was considered to denote low inflammation, whereas a score greater than 3 denoted high inflammation. Liver fibrosis was assessed using the Kleiner fibrosis stages, as has been described elsewhere [5, 26].

MR Elastography and MR Proton-Density Fat Fraction

MRI—MRI studies were performed using a 1.5-T scanner (Optima MR450w, GE Healthcare). All patients were instructed to avoid food and water for at least 4 hours before the examination. MR images were interpreted by one radiologist trained in abdominal fellowship who had 8 years of experience.

MR elastography—An acoustic passive driver was placed over the patients' right upper quadrant and was vibrated at 60 Hz. A 2D gradient-echo pulse sequence was used with the following parameters: an axial imaging plane; number of slices, 4; slice thickness, 8 mm; spacing, 5 mm; FOV, 42 cm^2; matrix, 256 × 64; number of excitations, 1; bandwidth, 31.25; TR/TE, 50/21.8; and flip angle, 30°. In addition, the shear-wave images were processed with an inversion algorithm to produce elastograms. ROIs were drawn over the slices, and the mean was calculated. Care was taken to exclude large hepatic vessels, the edge of the liver (which was considered one-half the width of a wave from the liver edge), and any areas of poor signal-to-noise ratio indicated on the elastogram and mask images when a phase and magnitude threshold of 5 was used.

MRI proton-density fat fraction—The MRI PDFF was determined using six gradient-echo breathhold pulse sequences (IDEAL IQ,

GE Healthcare) acquired using the following parameters: an axial imaging plane; slice thickness, 12 mm; spacing, 6 mm; FOV, 50 cm^2; matrix, 192 × 192; number of excitations, 0.68; TR/TE, 12.4/5.9; and flip angle, 7°. The PDFF was calculated by placing nine ROIs throughout the liver, with one ROI placed in each hepatic segment, and the mean was determined.

PET and Tracer Kinetic Modeling

Dynamic FDG PET—Dynamic FDG PET studies were performed using a PET/CT scanner (Discovery 690, GE Healthcare). Patients with diabetes were instructed to abstain from taking their morning dose of short-acting insulin, long-acting overnight dose of insulin, or both doses. The blood glucose level before PET was measured for all patients. Patients were positioned to allow the liver to be covered in the axial FOV (≈16 cm^2) of the PET/CT scanner. Each patient was injected with 370 MBq of FDG, in accordance with a routine clinical protocol. List-mode data acquisition was started right after the administration of the IV bolus and lasted for 1 hour. After PET was completed, a low-dose CT scan was obtained for attenuation correction for PET. The total effective radiation dose from the PET/CT scan was ≈7.5 mSv. The dynamic PET data were binned into 49 time frames by use of the following sampling schedule: 30 × 10 s, 10 × 60 s, and 9 × 300 s. Dynamic PET images were reconstructed using the vendor's software with use of the ordered-subsets expectation maximization algorithm.

Tracer kinetic modeling—Eight spherical ROIs, each 25 mm in diameter, were placed on the eight segments of the liver, with the caudate lobe excluded (Fig. 1A). These ROI placements were tuned and confirmed by an experienced abdominal radiologist. The time-activity curves of the eight ROIs were averaged to form a time-activity curve of the liver. An additional ROI was placed in the descending aorta region to extract the image-derived blood input function. We used an in-house kinetic modeling package to estimate the kinetic parameters on the basis of a well-established three-compartment model (Fig. 1B). The modeling algorithm also used an additional compartment to correct for the dispersion effect caused by the dual blood supply system in the liver (Fig. 1C). We measured four different microkinetic parameters that represent the FDG transport rate constant between compartments (FDG transport from blood to hepatic tissue [K_1], FDG transport from hepatic tissue to plasma [k_2], FDG phosphorylation into FDG 6-phosphate by hexokinase in cells [k_3], and FDG dephosphorylation [k_4]) (Fig. 1A) and a macrokinetic parameter that indicates the overall FDG net influx rate (K_i), where $K_i = K_1 \times [k_3 / (k_2 + k_3)]$. The SUV at 1 hour after FDG injection was also calculated using the standard formula. The SUV ratio was calculated as the ratio of the liver SUV to the blood SUV, to adjust for body factors.

Statistical Analysis

Sample size—A sample size of 22 patients provides 85% power to detect a correlation of 0.6 as well as 80% power to detect an effect size of 1.5-SD difference between group mean values, at the 0.05 level (two-sided). Pearson correlation coefficients for the association between kinetic parameters and both the hepatic inflammation score and the NAS score, in addition to their 95% CIs, were calculated. To compare the kinetic parameters in patients with low (grade, ≤ 3) and high (grade, > 3) inflammation or a low (grade, ≤ 4) or high (grade, > 4) NAS score, mixed-effects models with a random intercept for the patient were used. To assess the association between K_1 and high inflammation versus low inflammation and a high NAS score versus a low NAS score, we estimated the ROC AUC curve using logistic regression, as well as the sensitivity and specificity of an approximately optimal K_1 cutpoint. The clinical characteristics of the patients were expressed as frequencies and percentages or means and SDs, as appropriate. All statistical analyses were conducted using either Matlab (version 2017a, MathWorks) or SAS software (version 9.3, SAS Institute), and graphs were generated using Prism 7 (GraphPad). Statistical significance was assessed at the 0.05 level (two-sided).

Results

Patient Characteristics

Twenty-two patients who were undergoing liver biopsy were enrolled, and all underwent dynamic FDG PET and MRI (MRI PDFF and MRE). The mean interval from liver biopsy to PET and MRI was 8.1 ± 4.1 weeks. Table 1 shows the demographic and biochemical characteristics of the patients at baseline. In brief, most patients were white or Hispanic (90%), 64% were women, and more than three-quarters of the patients were 40–70 years of age, with age ranging from 18 to 70 years among the cohort. The mean BMI was 33.2 ± 5.2 (range, 24–43.1), and the mean waist circumference was 108.9 ± 11.3 cm (range, 88–127 cm). Seven of the patients had diabetes mellitus, 10 had hypertension, and seven had hyperlipidemia, with two patients having all three conditions. Eight patients were taking metformin (one patient who did not have diabetes but was taking metformin for presumed hyperinsulinemia), and none were taking insulin. The mean fasting glucose level before PET was performed was 116 ± 33 mg/dL (range, 83–202 mg/dL). Table 1 shows the histopathologic characteristics of the patients. Although most patients had steatosis of grade 2 or 3, distribution of hepatic inflammation scores (grade, ≤ 3 or > 3) and fibrosis scores was equitable. The internal validity of the biopsy readings was tested by correlation with MRI PDFF and MRE scores because these values were well established [24]. As shown in Fig. S1 (a supplemental figure, which can viewed in the *AJR* electronic supplement to this article, available at www.ajronline.org), significant correlation was noted between histopathologic scores for steatosis ($r = 0.7627$; $p < 0.0001$) and fibrosis ($r = 0.7703$; $p = 0.0001$), compared with MRI PDFF (expressed as percentage fat fraction) and MRE value (expressed as kilopascals), respectively.

FDG Microkinetics and Liver Inflammation

As noted in the Materials and Methods section, Figure 1B shows the three-compartment model of FDG transport kinetics between plasma and the intracellular milieu. K_1 significantly correlated with the hepatic inflammation score ($r = –0.7284$; $p = 0.0001$) (Fig. 1D). K_1 was also noted to correlate significantly with the overall NAS score ($r = –0.675$; $p = 0.0006$) (Fig. 1E). K_1 values were inversely related to hepatic inflammation and NAS. As shown in Table 2 and Fig. S2 (a supplemental figure, which can viewed in the *AJR* electronic supplement to this article, available at www.ajronline.org), the kinetic parameters k_3 ($r = 0.1114$; $p = 0.6215$) or k_4 ($r = –0.1529$; $p = 0.4970$) did not correlate with hepatic inflammation. In addition, no correlation of K_i ($r = 0.0305$; $p = 0.8929$) or SUV ($r = 0.1325$; $p = 0.5566$) with histologic hepatic inflammation was noted. Weak correlation was noted between k_2 and hepatic inflammation ($r = –0.5048$; $p = 0.0382$) between K_2 and NAS ($r = –0.4325$; $p = 0.0444$).

ROC Analysis

K_1 had a strong association with both inflammation (ROC AUC value, 0.88) and the NAS score (ROC AUC value, 0.89), as is shown in Figure 2. A cutpoint of $K_1 = 0.94$ mL/min/mL corresponded to sensitivity of 78% and specificity of 85% for detection of hepatic inflammation, whereas $K_1 = 1.02$ mL/min/mL corresponded to sensitivity and specificity of 93% and 88%, respectively, for the NAS score.

Segmental Heterogeneity in Glucose Transport

Distribution of disease in patients with NASH is believed to be heterogeneous [8, 29, 30]. Thus, we evaluated the heterogene-

TABLE 1: Baseline Demographic, Biochemical, and Histologic Characteristics of 22 Patients

Characteristic	No. (%) of Patients
Age (y)	
18–39	4 (18)
≥ 40–69	16 (73)
≥ 70	2 (9)
Sex	
Male	8 (36)
Female	14 (64)
Race or ethnicity	
White	14 (64)
Hispanic	6 (27)
Other	2 (9)
Body mass index[a]	
≤ 24.9	2 (9)
25–29.9	4 (18)
30–39.9	14 (64)
≥ 40	2 (9)
Waist circumference (cm)	
< 102	7 (32)
≥ 102	15 (68)
Alanine aminotransferase level	
< 40	7 (32)
40–120	11 (50)
> 120	4 (18)
Diabetes mellitus	
Present	7 (32)
Absent	15 (68)
Fasting blood glucose level before PET (mg/dL)	
< 100	8 (36)
100–125	10 (46)
> 125	4 (18)
NAFLD fibrosis score	
< –1.455	2 (9)
–1.455 to 0.675	7 (32)
> 0.675	13 (59)
Steatosis grade	
0 or 1	7 (32)
2 or 3	15 (68)
Inflammation score[b]	
≤ 3	13 (59)
> 3	9 (41)
Kleiner fibrosis stage	
0, 1a, or 1b	13 (59)
2, 3, or 4	9 (41)
NAFLD activity score	
0–4	8 (36)
5–8	14 (64)

Note—NAFLD = nonalcoholic fatty liver disease.
[a]Weight in kilograms divided by the square of height in meters.
[b]Lobular inflammation plus ballooning degeneration (scores of 0–5).

ity of K_1 values across the eight liver segments measured. Figure 3A shows representative images of three patients with increasing histologic inflammation scores in which heterogeneity in FDG uptake is visualized between the segments. Quantitative K_1 values were noted to be variable between segments among the individual patients (median variation between segments, 0.15 mL/min/mL; range, 0.05–0.29 mL/min/mL). Figure 3B shows the mean (plus or minus variation) in K_1 among the eight segments in each of the 22 patients. When the patients were segregated on the basis of their histologic inflammation scores (with low inflammation denoted by a score ≤ 3 and high inflammation by a score > 3), a distinct pattern of FDG uptake was noted. The mean and median (range) of K_1 values for the low inflammation group were 1.1139 ± 0.21 mL/min/mL and 1.1220 mL/min/mL (0.7681–1.2926 mL/min/mL), respectively, compared with those for patients with high inflammation, for whom the mean was 0.8318 ± 0.14 mL/min/mL and the median (range) was 0.83 mL/min/mL (0.6203–1.0038 mL/min/mL). The K_1 scores in each of the segments are shown in Table 3 and revealed an overall decrease in K_1 as NASH progressed. Of note, a distinct segregation existed among those with low or high inflammation (Fig. 3C) ($p = 0.022$), and this was also noted when patients were segregated on the basis of NAS (with a low NAS of ≤ 4 and a high NAS of > 4) (Fig. 3D) ($p = 0.0091$).

Discussion

With the use of dynamic FDG PET and advanced tracer kinetic modeling, and with the dual blood supply in the liver taken into consideration, we exploited the kinetic characteristics of glucose metabolism and quantified the fundamental molecular process underlying hepatic glucose utilization on a regional basis. Using these methods, we present a study of FDG PET uptake kinetics in the liver as a potential tool for determining changes in hepatic inflammation in patients with nonalcoholic steatohepatitis in correlation with liver biopsy. Excellent work by various groups over the past decade has established FDG PET in the study of the physiologic liver processes affected in metabolic diseases such as obesity and NAFLD [16, 31–34]. As previously noted, Borra et al. [20] studied the association of liver fat and hepatic glucose uptake and found an inverse relationship. Abikhzer et al. [35] and Lin et al. [36] also reported a small negative correlation of FDG SUV with hepatic steatosis. However, it was necessary to determine FDG PET changes in correlation with liver biopsy to measure the disease state.

Dissecting the steps of the glucose uptake pathway enabled characterization in relation to histopathologic changes in NAFLD. This

TABLE 2: Summary of FDG Kinetic Parameters and Correlation With Hepatic Inflammation and Nonalcoholic Fatty Liver Disease Activity Score (NAS)

FDG Kinetic Parameter	Hepatic Inflammation		NAS	
	r	*p*	*r*	*p*
K_1	−0.7284	0.0001[a]	−0.675	0.0006[a]
k_2	−0.5048	0.0382[a]	−0.4325	0.0444[a]
k_3	0.1114	0.6215	0.148	0.5109
k_4	−0.1529	0.4970	−0.0851	0.7066
K_i	−0.0305	0.8929	−0.02384	0.9161
SUV	0.1325	0.5566	0.0663	0.7693

Note—K_1 = rate of FDG transport from blood to hepatic tissue, k_2 = rate of FDG transport from blood to hepatic tissue to plasma, k_3 = the rate of phosphorylation, k_4 = the rate of dephosphorylation, K_i = FDG net influx rate, SUV = standardized uptake value.
[a] $p < 0.01$.

TABLE 3: Segmental Rates of FDG Transport From Blood to Hepatic Tissue (K_1 Values, Unit: mL/min/mL) Segregated by Low and High Inflammation

Segmental K_1 Value	K_1 Value (mL/min/mL) of Patients With Low Inflammation (n = 13)[a]		K_1 Value (mL/min/mL) of Patients With High Inflammation (n = 9)[b]	
	Mean ± SD	Median (Range)	Mean ± SD	Median (Range)
Overall	1.1139 ± 0.21	1.122 (1.56–0.77)	0.8318 ± 0.14	0.8300 (1–0.62)
Segment 2	1.1126 ± 0.26	1.2136 (1.45–0.66)	0.8312 ± 0.18	0.8292 (1.22–0.55)
Segment 3	1.0070 ± 0.37	0.9365 (1.9–0.37)	0.8955 ± 0.18	0.8812 (1.15–0.58)
Segment 4A	1.0869 ± 0.22	1.0815 (1.42–0.72)	0.8849 ± 0.19	0.8381 (1.27–0.63)
Segment 4B	1.2358 ± 0.42	1.1118 (2.22–0.65)	0.8557 ± 0.23	0.7979 (1.30–0.62)
Segment 5	1.0372 ± 0.33	1.0046 (1.87–0.56)	0.7166 ± 0.12	0.7827 (0.83–0.49)
Segment 6	1.0642 ± 0.31	0.9992 (1.6–0.59)	0.8530 ± 0.17	0.9324 (1.03–0.61)
Segment 7	1.0830 ± 0.32	1.1965 (1.69–0.59)	0.9433 ± 0.15	0.9596 (1.17–0.73)
Segment 8	1.1552 ± 0.26	1.1901 (1.64–0.56)	−0.9244 ± 0.16	0.9130 (1.23–0.65)

Note—K_1 = rate of FDG transport from blood to hepatic tissue.
[a] Low inflammation denoted by a histologic inflammation score of 3 or less.
[b] High inflammation denoted by a histologic inflammation score greater than 3.

is one of the first studies to compare dynamic FDG PET findings with liver histologic findings. We note that, specifically, the first step in the uptake pathway, the transport of FDG from plasma to intracellular compartment (K_1), was significantly correlated with histologic inflammation. This correlation was also noted with the overall NAFLD activity score (NAS) for which a decrease in K_1 was associated with increased NAS scores. We hypothesize that a combination of insulin resistance, increased intrahepatic fat (presumably resulting in decreased liver blood flow), and disease progression with fibrous tissue deposition, collagen deposition, or both [31, 37] leads to the decrease in K_1 with worsening of the disease state. The parameter k_3, which is representative of phosphorylation, increased with a change in inflammation, although this finding remains nonsignificant. An increase in the glucose phosphorylation rate has been noted with increased steatosis [17], and it can be affected by insulin sensitivity [18], although the disease correlate of this remains unclear at present. Data for a larger and more diverse cohort of patients and an improvement in methods will add to the definition of the kinetic pathway, helping to elucidate the effect of progression of NASH on FDG transport kinetics.

It is essential to consider that FDG uptake may be affected by changes in insulin sensitivity or exogenous insulin administration [18, 21, 38]. Our protocol called for control of exogenous insulin by abstain from taking their overnight dose of long-acting insulin, morning dose of short-acting insulin, or both doses, although none of the patients in this cohort were taking insulin. Eight patients (seven patients with diabetes and one with apparent hyperinsulinemia) were taking metformin, and their K_1 values were unaffected; however, these numbers are low for statistical relevance.

In view of studies showing perceived heterogeneity of the liver [8, 29, 30], especially as noted in diseases such as NAFLD and NASH, we measured the kinetics in eight of the liver segments (all segments except the caudate lobe). We found two key aspects that we presented in this study. First, heterogeneity of FDG uptake kinetics was noted across the segments of the liver. This shows the ability of FDG PET to determine changes in glucose uptake in each segment of the entire liver and, moreover, conforms with the known histologic heterogeneity of NASH [8, 29, 30]. Each patient had a unique variability pattern. This variability may very well be affected by diurnal changes or other extraneous factors that can affect FDG uptake. It is also possible that the heterogeneity is, at least in part, caused by differences in the vascular supply, because each segment showed a distinct pattern of uptake kinetics. Second, although heterogeneity existed for the patients, the mean K_1 values for each segment when analyzed on the basis of high- or low- inflammation groups and high- or low- NAS groups showed that FDG uptake clearly depended on the level of inflammation. This finding suggests that although heterogeneity exists, a similar trajectory of disease worsening and inflammation is noted as the disease progresses across all the liver segments.

A few limitations of the present study are essential to consider. This is a small single-center study. Therefore, it limits the ability to conclusively determine the benefit of this noninvasive test. This study is meant to provide data that will help lay the foundation for future utilization of dynamic FDG PET with tracer kinetic modeling to diagnose, quantify, and potentially monitor steatohepatitis. Furthermore, patients are exposed to additional radiation from the PET/CT examination. However, the radiation risk associated with this method remains minimal, and the total effective radiation dose from the dynamic liver PET/CT method is approximately 7.5 mSv. This is equivalent to 2.5 years of natural background radiation and is lower than the total effective radiation dose from the whole-body FDG PET/CT examination (≈11 mSv) [39]. This study focuses on the efficacy of the method, and our future

studies will be targeted to use even lower doses of FDG to acquire relevant data. The current cost of PET/CT is approximately $1500 per scan and is comparable to the cost of liver biopsy (approximately $1500–2200), but this cost is lower in terms of the relative complications experienced by patients and subsequent associated costs. Future costs of PET scans may actually decrease once the method is well established and its use is more widespread.

In sum, in this proof-of-concept study, we presented dynamic FDG PET as a potential tool for the detection and quantitation of changes in hepatic inflammation. The study provides an imaging tool with which to determine the presence of NASH without the need for liver biopsy in patients for whom clinical indicators and imaging findings raise the question of intermediate disease stages. We believe that with advances in methods and technology, the scanning time will significantly shorten and the radiation dose will further decrease. Such advancements and the development of a whole-body PET scanner (Explorer, developed by University of California, Davis; Berkeley Lab; and the University of Pennsylvania) can potentially allow monitoring of affected patients in the future. This also has the potential for utilization as a surrogate clinical endpoint in conjunction with other modalities in future clinical studies, in addition to its use in determining physiologic changes in the entire liver with therapeutic interventions.

Acknowledgments

We thank our patients for participating in the study. We also thank Conjing (Ella) Zha and Cole Johnson, for their assistance in patient enrollment, and Heather Hunt, Michael Rusnak, Mike Nguyen, Benjamin Spencer, and Denise Caudle, for their assistance in PET/CT data acquisition.

References

1. Rinella ME. Nonalcoholic fatty liver disease: a systematic review. *JAMA* 2015; 313:2263–2273
2. Loomba R, Sanyal AJ. The global NAFLD epidemic. *Nat Rev Gastroenterol Hepatol* 2013; 10:686–690
3. Angulo P, Kleiner DE, Dam-Larsen S, et al. Liver fibrosis, but no other histologic features, is associated with long-term outcomes of patients with nonalcoholic fatty liver disease. *Gastroenterology* 2015; 149:389.e10–397.e10
4. Chalasani N, Younossi Z, Lavine JE, et al. The diagnosis and management of nonalcoholic fatty liver disease: practice guidance from the American Association for the Study of Liver Diseases. *Hepatology* 2018; 67:328–357
5. Kleiner DE, Brunt EM. Nonalcoholic fatty liver disease: pathologic patterns and biopsy evaluation in clinical research. *Semin Liver Dis* 2012; 32:3–13
6. Satapathy SK, Sanyal AJ. Epidemiology and natural history of nonalcoholic fatty liver disease. *Semin Liver Dis* 2015; 35:221–235
7. Brown GT, Kleiner DE. Histopathology of nonalcoholic fatty liver disease and nonalcoholic steatohepatitis. *Metabolism* 2016; 65:1080–1086
8. Ratziu V, Charlotte F, Heurtier A, et al. Sampling variability of liver biopsy in nonalcoholic fatty liver disease. *Gastroenterology* 2005; 128:1898–1906
9. Loomba R, Sirlin CB, Ang B, et al. Ezetimibe for the treatment of nonalcoholic steatohepatitis: assessment by novel magnetic resonance imaging and magnetic resonance elastography in a randomized trial (MOZART trial). *Hepatology* 2015; 61:1239–1250
10. Filozof C, Goldstein BJ, Williams RN, Sanyal A. Non-alcoholic steatohepatitis: limited available treatment options but promising drugs in development and recent progress towards a regulatory approval pathway. *Drugs* 2015; 75:1373–1392
11. Yilmaz Y. Biomarkers for early detection of nonalcoholic steatohepatitis: implications for drug development and clinical trials. *Curr Drug Targets* 2013; 14:1357–1366
12. Gambhir SS. Molecular imaging of cancer with positron emission tomography. *Nat Rev Cancer* 2002; 2:683–693
13. Ben-Haim S, Ell P. ^{18}F-FDG PET and PET/CT in the evaluation of cancer treatment response. *J Nucl Med* 2009; 50:88–99
14. Boellaard R, Delgado-Bolton R, Oyen WJG, et al. FDG PET/CT: EANM procedure guidelines for tumour imaging—version 2.0. *Eur J Nucl Med Mol Imaging* 2015; 42:328–354
15. Abele JT, Fung CI. Effect of hepatic steatosis on liver FDG uptake measured in mean standard uptake values. *Radiology* 2010; 254:917–924
16. Keiding S. Bringing physiology into PET of the liver. *J Nucl Med* 2012; 53:425–433
17. Keramida G, Hunter J, Peters AM. Hepatic glucose utilization in hepatic steatosis and obesity. *Biosci Rep* 2016; 36(3):e00402
18. Iozzo P, Geisler F, Oikonen V, et al. Insulin stimulates liver glucose uptake in humans: an ^{18}F-FDG PET study. *J Nucl Med* 2003; 44:682–689
19. Schmidt KC, Turkheimer FE. Kinetic modeling in positron emission tomography. *Q J Nucl Med* 2002; 46:70–85
20. Borra R, Lautamaki R, Parkkola R, et al. Inverse association between liver fat content and hepatic glucose uptake in patients with type 2 diabetes mellitus. *Metabolism* 2008; 57:1445–1451
21. Iozzo P, Hallsten K, Oikonen V, et al. Effects of metformin and rosiglitazone monotherapy on insulin-mediated hepatic glucose uptake and their relation to visceral fat in type 2 diabetes. *Diabetes Care* 2003; 26:2069–2074
22. Barton GP, Vildberg L, Goss K, Aggarwal N, Eldridge M, McMillan AB. Simultaneous determination of dynamic cardiac metabolism and function using PET/MRI. *J Nucl Cardiol* 2018 May 1 [Epub ahead of print]
23. Wang G, Corwin MT, Olson KA, Badawi RD, Sarkar S. Dynamic PET of human liver inflammation: impact of kinetic modeling with optimization-derived dual-blood input function. *Phys Med Biol* 2018; 63:155004
24. Noureddin M, LAm J, Peterson MR, et al. Utility of magnetic resonance imaging versus histology for quantifying changes in liver fat in nonalcoholic fatty liver disease trials. *Hepatology* 2013; 58:1930–1940
25. Loomba R, Wolfson T, Ang B, et al. Magnetic resonance elastography predicts advanced fibrosis in patients with nonalcoholic fatty liver disease: a prospective study. *Hepatology* 2014; 60:1920–1928
26. Brunt EM, Kleiner DE, Wilson LA, Belt P, Neuschwander-Tetri BA; NASH Clinical Research Network. Nonalcoholic fatty liver disease (NAFLD) activity score and the histopathologic diagnosis in NAFLD: distinct clinicopathologic meanings. *Hepatology* 2011; 53:810–820
27. Kleiner DE, Brunt EM, Van Natta M, et al. Design and validation of a histological scoring system for nonalcoholic fatty liver disease. *Hepatology* 2005; 41:1313–1321
28. Yeh MM, Brunt EM. Pathological features of fatty liver disease. *Gastroenterology* 2014; 147:754–764
29. Larson SP, Bowers SP, Palekar NA, Ward JA, Pulcini JP, Harrison SA. Histopathologic variability between the right and left lobes of the liver in morbidly obese patients undergoing Roux-en-Y bypass. *Clin Gastroenterol Hepatol* 2007; 5:1329–1332
30. Merriman RB, Ferrell LD, Patti MG, et al. Correlation of paired liver biopsies in morbidly obese patients with suspected nonalcoholic fatty liver disease. *Hepatology* 2006; 44:874–880
31. Bechmann LP, Hannivoort RA, Gerken G, Hotamisligil GS, Trauner M, Canbay A. The interaction of hepatic lipid and glucose metabolism in liver diseases. *J Hepatol* 2012; 56:952–964
32. Brix G, Ziegler SI, Bellemann ME, et al. Quantification of [^{18}F]FDG uptake in the normal liver using dynamic PET: impact and modeling of the dual hepatic blood supply. *J Nucl Med* 2001; 42:1265–1273

33. Iozzo P, Bucci M, Roivainen A, et al. Fatty acid metabolism in the liver, measured by positron emission tomography, is increased in obese individuals. *Gastroenterology* 2010; 139:846–856, 856.e1–856.e6
34. Trägårdh M, Møller N, Sørensen M. Methodologic considerations for quantitative ^{18}F-FDG PET/CT studies of hepatic glucose metabolism in healthy subjects. *J Nucl Med* 2015; 56:1366–1371
35. Abikhzer G, Alabed YZ, Azoulay L, Assayag J, Rush C. Altered hepatic metabolic activity in patients with hepatic steatosis on FDG PET/CT. *AJR* 2011; 196:176–180
36. Lin CY, Lin WY, Lin CC, Shih CM, Jeng LB, Kao CH. The negative impact of fatty liver on maximum standard uptake value of liver on FDG PET. *Clin Imaging* 2011; 35:437–441
37. Hernandez-Martinez A, Marin-Oyaga VA, Salavati A, et al. Quantitative assessment of global hepatic glycolysis in patients with cirrhosis and normal controls using ^{18}F-FDG-PET/CT: a pilot study. *Ann Nucl Med* 2014; 28:53–59
38. Gastaldelli A, Gaggini M, Daniele G, et al. Exenatide improves both hepatic and adipose tissue insulin resistance: a dynamic positron emission tomography study. *Hepatology* 2016; 64:2028–2037
39. Radiological Society of North America. Radiation dose in x-ray and CT exams. RadiologyInfo.org website. www.radiologyinfo.org/en/info.cfm?pg=safety-xray. Published 2016. Accessed October 31, 2018

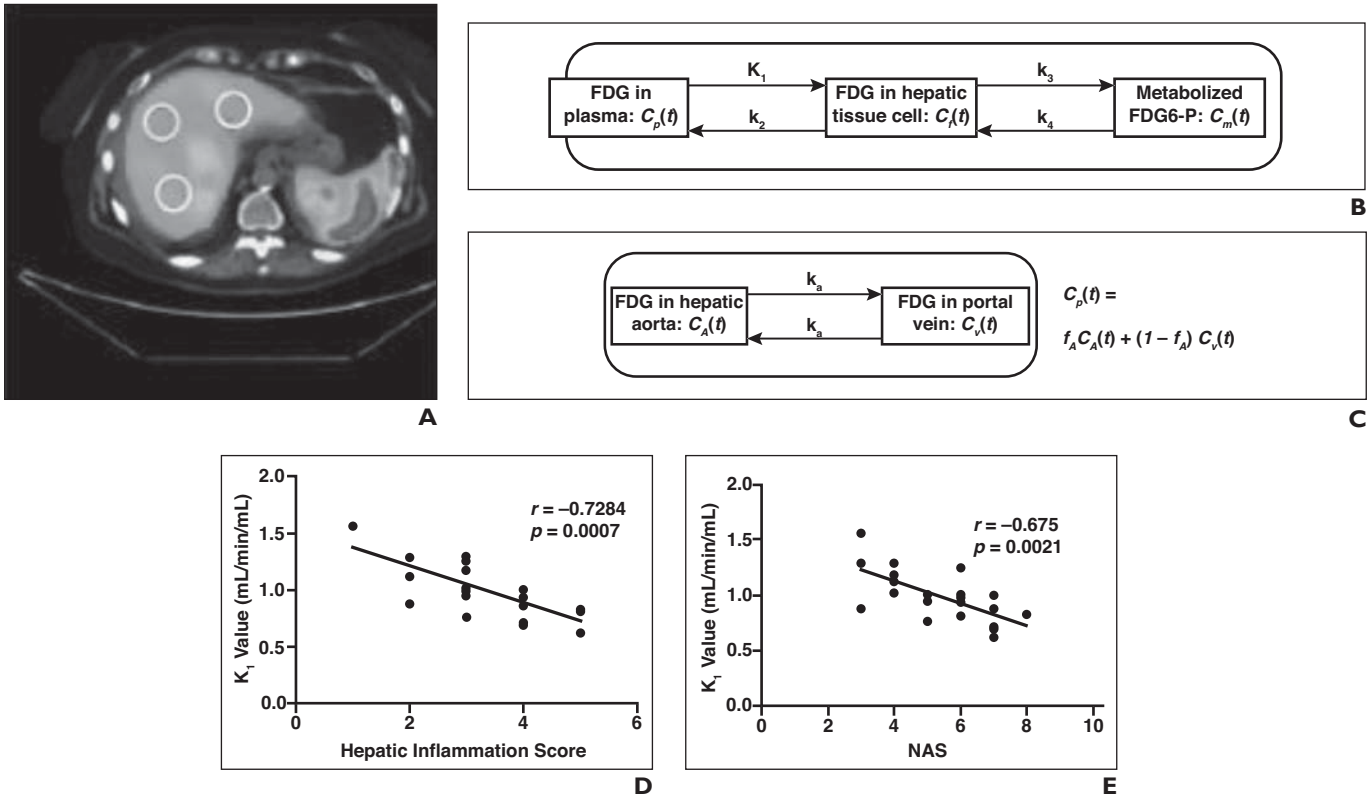

Fig. 1—Dynamic FDG PET kinetic parameters and hepatic inflammation.
A, 38-year-old woman with nonalcoholic fatty liver disease. Dynamic FDG PET image of transport of FDG from plasma to intracellular compartment (K_1) with three representative ROIs (*circles*) (of eight total ROIs).
B, Diagram of three-compartment model of FDG transport from plasma to hepatic tissue with rate constant (K_1 value; expressed as milliliters per minute per milliliter) and from hepatic tissue to plasma (k_2 value, which is expressed as fraction of mass transferred per minute [min^{-1}]). FDG is phosphorylated by hexokinase in cells into FDG 6-phosphate (k_3 value, which is expressed as fraction of mass transferred per minute [min^{-1}]) and also dephosphorylated (k_4 value, which is expressed as fraction of mass transferred per minute [min^{-1}]). k_2 = FDG transport from hepatic tissue to plasma, k_3 = FDG phosphorylation into FDG 6-phosphate by hexokinase in cells, k_4 = FDG dephosphorylation, $C_p(t)$ = concentration of FDG in plasma, $C_f(t)$ = free-state FDG in tissue, $C_m(t)$ = metabolized FDG 6-phosphate in tissue.
C, Diagram of overall blood input function modeled as dual blood contribution from both hepatic artery and portal vein. Aortic input is derived from dynamic PET images, and portal vein input is estimated during kinetic parameter estimation. Portal vein input is modeled as function of time (t): $C_V(t) = k_a \exp(-k_a t) * C_A(t)$, where * denotes time convolution, $k_a t$ denotes dispersion rate from arteries to portal vein, and $C_A(t)$ denotes concentration of FDG in hepatic artery. Parameters f_A (denoting fraction of hepatic artery contributing to overall blood flow) and k_a (denoting dispersion rate from arteries to portal vein) are jointly estimated with other compartmental model parameters. $C_p(t)$ denotes overall concentration of FDG in plasma.
D and **E,** Graphs of correlation of rate of FDG transport from blood to hepatic tissue (K_1 value) with hepatic inflammation score **(D)** and overall nonalcoholic fatty liver disease activity score (NAS) **(E)**. Circles denote individual patient's K_1 values, and diagonal line denotes slope.

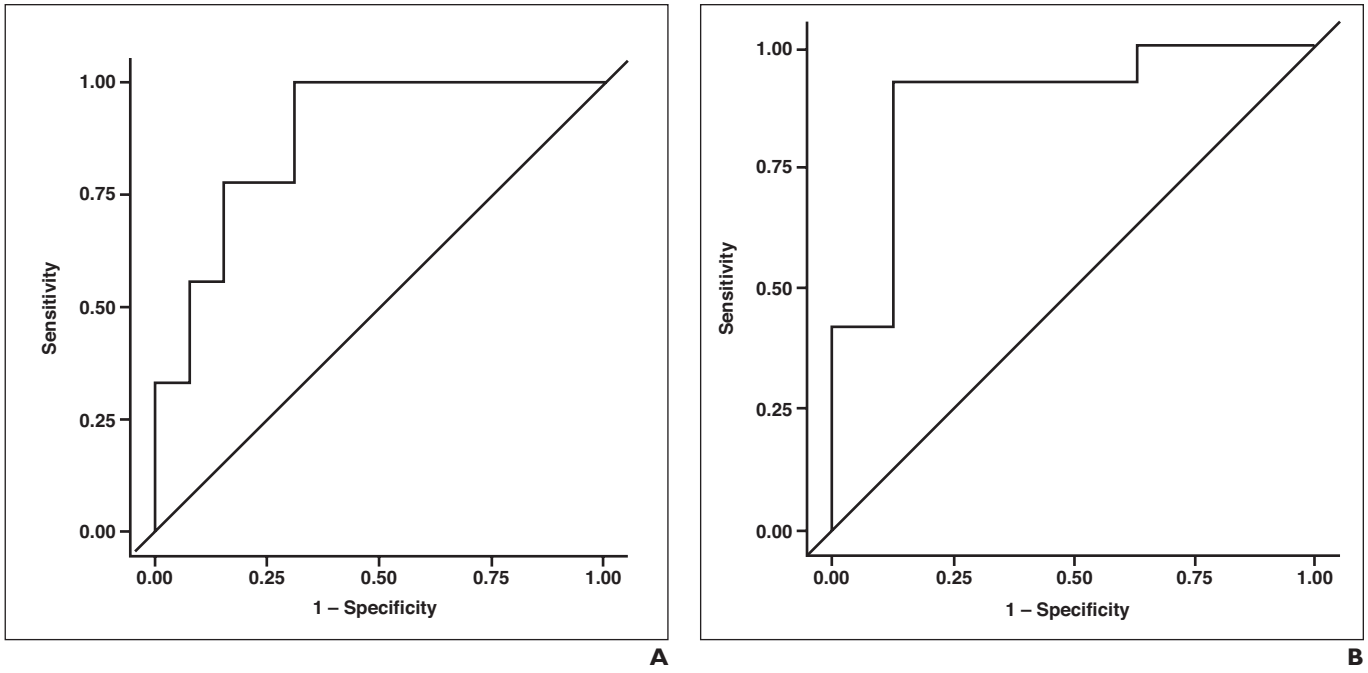

Fig. 2—ROC AUC curve analyses of associations with rate of FDG transport from blood to hepatic tissue (K_1), as performed using logistic regression. Black line denotes ROC AUC curve, and diagonal line denotes reference.
A, ROC AUC curve of association between K_1 and high versus low inflammation (ROC AUC value, 0.8803).
B, ROC AUC curve of association between K_1 and high versus low nonalcoholic fatty liver disease activity score (ROC AUC value, 0.8929).

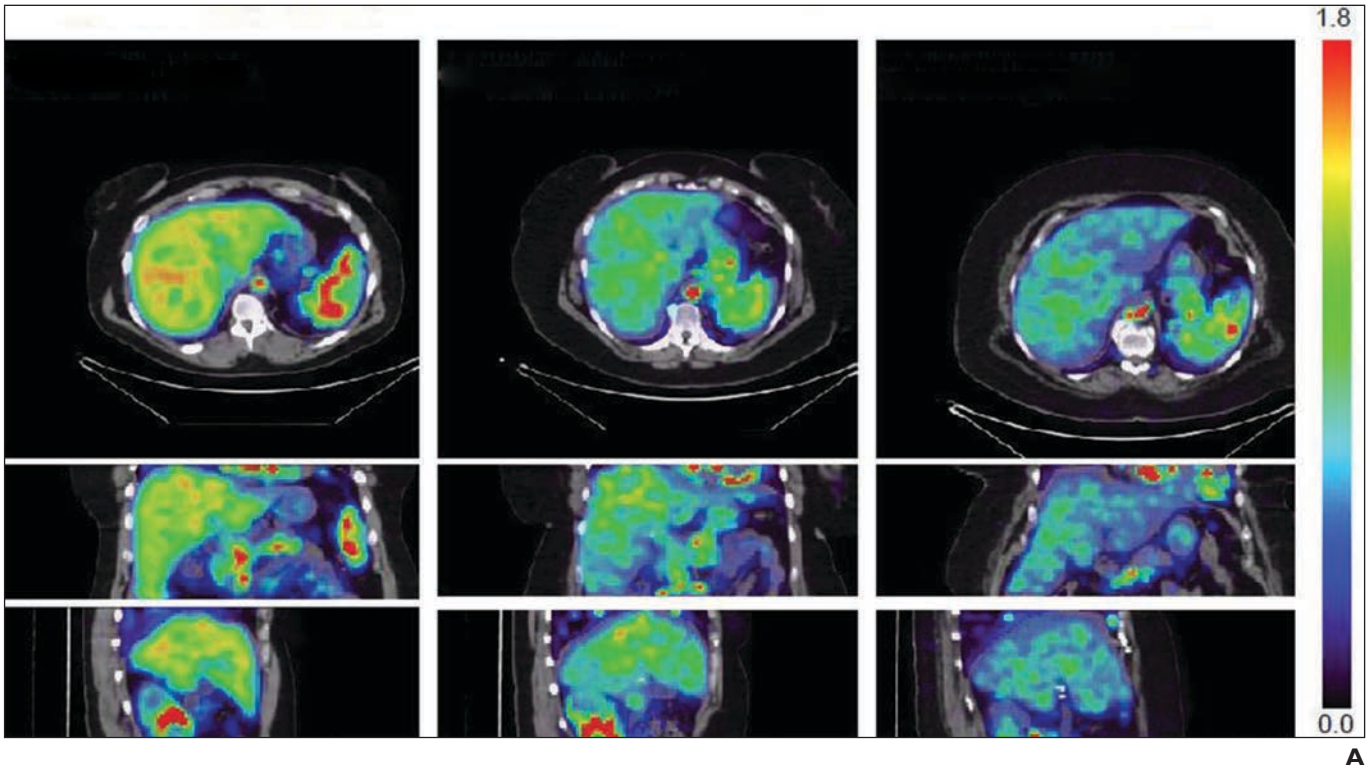

Fig. 3—Distribution of rates of FDG transport from blood to hepatic tissue (K_1) across liver segments.
A, Representative PET images of K_1 distribution in patients with histologic hepatic inflammation scores of 1 (mean liver K_1 value, 1.29 mL/min/mL) (38-year-old man with with nonalcoholic fatty liver disease) (*left column*), 3 (mean liver K_1 value, 0.83 mL/min/mL) (50-year-old woman with nonalcoholic steatohepatitis [NASH]) (*middle column*), and 5 (mean liver K_1 value, 0.60 mL/min/mL) (54-year-old woman with NASH) (*right column*).

(Fig. 3 continues on next page)

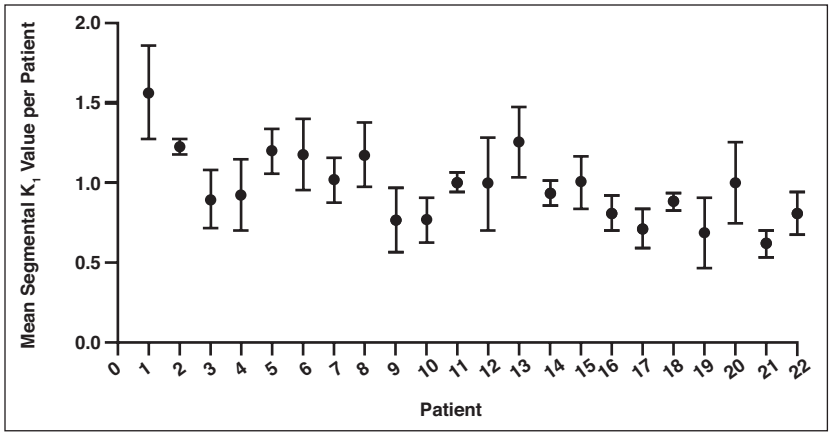

B

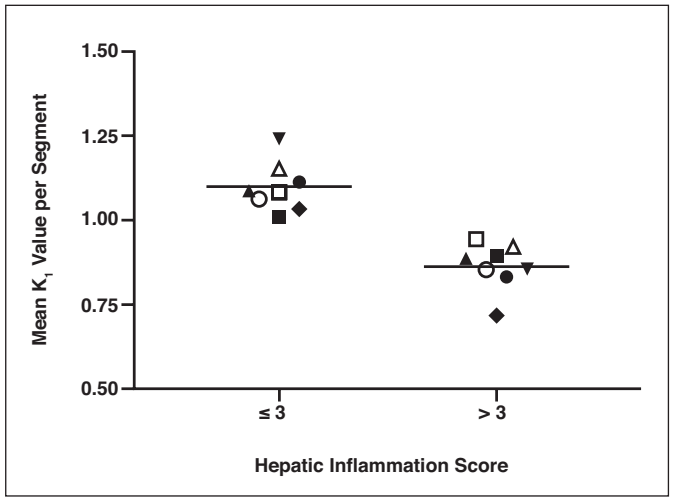

C

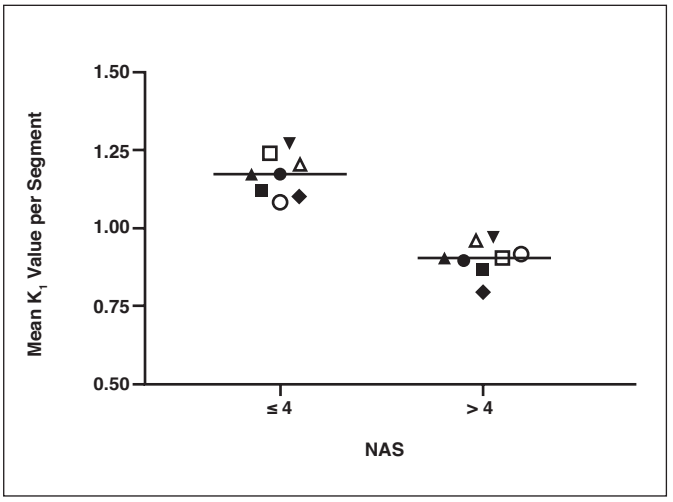

D

Fig. 3 (continued)—Distribution of rates of FDG transport from blood to hepatic tissue (K_1) across liver segments.
B, Graph of mean (± SD) K_1 values for eight segments from each patient. Circles on horizontal lines denote mean value for each patient, and whiskers denote SDs.
C and **D,** Mean K_1 values per segment, as segregated on basis of low-to-moderate or high inflammation scores ($p = 0.022$) (**C**) and low or high nonalcoholic fatty liver disease activity scores (NAS) ($p = 0.0091$) (**D**). Open circles denote segment 6; open squares, segment 7; open triangles, segment 8; solid circles, segment 2; solid squares, segment 3; upright solid triangles, segment 4A; inverted solid triangles, segment 4B; and solid diamonds, segment 5. Horizontal lines denote mean values.

FOR YOUR INFORMATION

A data supplement for this article can be viewed in the online version of the article at: www.ajronline.org.